REPORT DOCUMENTATION PAGE

1a. REPORT SECURITY CLASSIFICATION
UNCLASSIFIED

1b. RESTRICTIVE MARKINGS

2a. SECURITY CLASSIFICATION AUTHORITY

3. DISTRIBUTION/AVAILABILITY OF REPORT

2b. DECLASSIFICATION/DOWNGRADING SCHEDULE

Approved for public release; distribution is unlimited.

4. PERFORMING ORGANIZATION REPORT NUMBER(S)

5. MONITORING ORGANIZATION REPORT NUMBER(S)

6a. NAME OF PERFORMING ORGANIZATION
Naval Postgraduate School

6b. OFFICE SYMBOL (*If applicable*)
61

7a. NAME OF MONITORING ORGANIZATION
Naval Postgraduate School

6c. ADDRESS (*City, State, and ZIP Code*)
Monterey, CA 93943-5000

7b. ADDRESS (*City, State, and ZIP Code*)
Monterey, CA 93943-5000

8a. NAME OF FUNDING/SPONSORING ORGANIZATION

8b. OFFICE SYMBOL (*If applicable*)

9. PROCUREMENT INSTRUMENT IDENTIFICATION NUMBER

8c. ADDRESS (*City, State, and ZIP Code*)

10. SOURCE OF FUNDING NUMBERS

Program Element No	Project No.	Task No.	Work Unit Accession Number

11. TITLE (*Include Security Classification*)
Investigation of Thermoacoustic Muffler

12. PERSONAL AUTHOR(S) Che, Chun-Hua

13a. TYPE OF REPORT	13b. TIME COVERED		14. DATE OF REPORT (*year, month, day*)	15. PAGE COUNT
Master's Thesis	From	To	December 1992	40

16. SUPPLEMENTARY NOTATION
The views expressed in this thesis are those of the author and do not reflect the official policy or position of the Department of Defense or the U.S. Government.

17. COSATI CODES

FIELD	GROUP	SUBGROUP

18. SUBJECT TERMS (*continue on reverse if necessary and identify by block number*)
Muffler Geometry, Thermoacoustic Prime Mover, Finite-Amplitude Standing Wave, Quality Factor, Temperature Difference

19. ABSTRACT (*continue on reverse if necessary and identify by block number*)

The design, construction and testing of a thermoacoustic muffler is discussed. The performance of the muffler is characterized by measuring its ability to reduce the quality factor Q of an acoustic resonator. Measurements of the Q of a helium filled muffler were made for temperature differences ranging from 0 to -130° C. The measured Q-reduction, approximately 30%, agrees with predicted reductions. The predictions are based on a standing wave analysis of thermoacoustic engines published by Atchley [J. Acoust. Soc. Am. 92, 2907-2914 (1992)]. These results indicate that Q-reduction is possible. Future work should concentrate on optimization, to determine of a thermoacoustic muffler is, in fact, practical.

20. DISTRIBUTION/AVAILABILITY OF ABSTRACT
☒ UNCLASSIFIED/UNLIMITED ☐ SAME AS REPORT ☐ DTIC USERS

21. ABSTRACT SECURITY CLASSIFICATION
UNCLASSIFIED

22a. NAME OF RESPONSIBLE INDIVIDUAL
A. A. Atchley

22b. TELEPHONE (*Include Area code*)
(408)656-2848

22c. OFFICE SYMBOL
61Ay

DD FORM 1473, 84 MAR

83 APR edition may be used until exhausted
All other editions are obsolete

SECURITY CLASSIFICATION OF THIS PAGE
UNCLASSIFIED

Approved for public release; distribution is unlimited.

INVESTIGATION OF THERMOACOUSTIC MUFFLER

by

Che, Chun-Hua
Commander, R. O. C. Navy
B.S., R.O.C. Naval Academy, 1978

Submitted in partial fulfillment
of the requirements for the degree of

MASTER OF SCIENCE IN ENGINEERING ACOUSTICS

from the

NAVAL POSTGRADUATE SCHOOL
December 1992

ABSTRACT

The design, construction and testing of a thermoacoustic muffler is discussed. The performance of the muffler is characterized by measuring its ability to reduce the quality factor Q of an acoustic resonator. Measurements of the Q of a helium filled muffler were made for temperature differences ranging from 0 to -130°C. The measured Q-reduction, approximately 30%, agrees with predicted reductions. The predictions are based on a standing wave analysis of thermoacoustic engines published by Atchley [J. Acoust. Soc. Am. 92, 2907-2914 (1992)]. These results indicate that Q-reduction is possible. Future work should concentrate on optimization, to determine of a thermoacoustic muffler is, in fact, practical.

TABLE OF CONTENTS

LIST OF FIGURES

LIST OF TABLES

LIST OF SYMBOLS

c	sound speed
E_{ST}	stored energy
$\dot{E}$	dissipated acoustic power
f	frequency
f_0	measured resonance frequency
k	propagation constant
k_{amb}	propagation constant at ambient end
L	resonator length
L_{eff}	effective length
l	plate half-thickness
P_A	peak acoustic pressure amplitude
Q	quality factor
R	resonator radius
R_{rad}	radiation resistance
S	cross sectional area of fluid
T_m	equilibrium temperature
u	acoustic particle velocity
x	direction along sound propagation
y_0	plate half-spacing
ΔT	temperature difference

LIST OF SYMBOLS (CONTINUED)

∇T_m	gradient of equilibrium temperature
Δx	plate length
δT	temperature change of parcel due to acoustic pressure change
Π	perimeter
ρ_0	density
ω	angular frequency
ξ	displacement of parcel

ACKNOWLEDGMENTS

First, I would like to express my sincerely grateful to my advisors, Pr. Anthony A. Atchley and Dr. Felipe Gaitan for their guidance, support, encouragement and infinite patience, leading me with faith to accomplish this thesis. Next I thank George Jaksha, David Gardner and Nelson Castro for their enthusiasm help in conducting my experiment. Also I want to thank Kuo, Fan-Ming, Liu, Chao-Shih and Kuo, Yu-Heng who help me in typing this thesis.

Finally, I reserve my special thanks for my wife, Chia-Lin, for her moral support and company to finish the study at Naval Postgraduate School.

I. INTRODUCTION

Thermoacoustic heat transport is a process through which an acoustic field generates, or is generated from, a flow of heat. Like a conventional engine, a thermoacoustic engine can be configured as either type of classical heat engine - a heat pump (or refrigerator) or a prime mover. Thermoacoustic devices have a broad range of application including refrigerators, air conditioners, cryocoolers, sound sources, and thermal-to-electric generators. The purpose of this thesis is a preliminary investigation of a yet unexplored application of thermoacoustics - a thermoacoustic muffler.

The necessary background for this thesis can be explained with reference to Fig. 1 which shows the basic operation and construction of a thermoacoustic prime mover. In this example, a prime mover can be considered to be a closed, closed acoustic resonator comprised of five sections. A temperature gradient is applied across the prime mover stack via the hot and ambient heat exchangers. (The terms "hot" and "ambient" refer to the temperatures of the heat exchangers and the portions of resonator adjacent to them.) In typical applications, the prime mover stack and heat exchangers are parallel plates, spaced by a few thermal penetration depths and oriented such that the plates lie along the axis of the resonator. The hot and ambient sections are circular tubes — open at the heat exchanger end and closed at the other end. The net absorption coefficient of the prime mover is the sum of the thermal and viscous wall losses in each of the five sections. Attenuation in the gas is negligible. As the temperature difference (ΔT) imposed across the stack increases from zero, the thermal losses in the stack decrease and eventually become negative, representing gain. At a sufficiently high ΔT, the gain of the stack overcomes the remaining losses (the viscous losses in

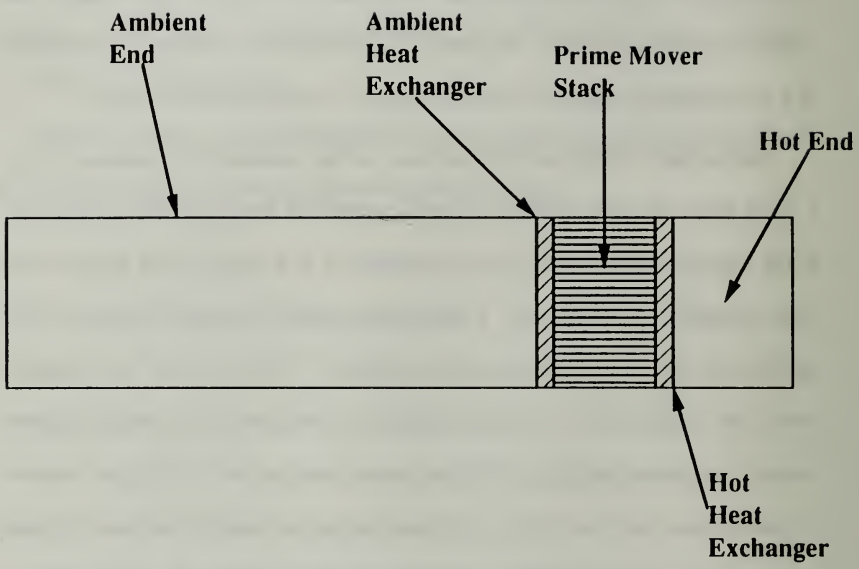

Figure 1 - Construction of thermoacoustic prime mover.

the stack and the thermal and viscous losses in the other four sections) and the prime mover spontaneously goes into self-oscillation. This phenomenon is known as onset.

The performance of a prime mover can be analyzed by measuring its quality factor Q. As ΔT increases, the net acoustic losses in the prime mover decrease resulting in a higher Q. This behavior is portrayed in Fig. 2, which shows the Q as a function of ΔT. Onset occurs when the Q diverges and becomes negative. Previous research [Refs. 1-3] has investigated prime movers both below and above onset. The solid line is the prediction of a standing wave analysis of thermoacoustic prime movers, published by Atchley [Ref. 3].

The question to be answered in this thesis is "What happens to Q if ΔT is negative?" The answer is "It goes down." This point is illustrated in Fig. 3, which shows a subset of the data from Fig. 2. In addition, the calculations have been extended for negative values of ΔT. For this prime mover, the Q can be reduced by a factor of approximately 2 from its value at $\Delta T = 0$ by applying a ΔT of -200 K, achievable with liquid nitrogen.

No measurements have been made in the negative ΔT region - the Q-reduction mode of operation. The purpose of this thesis is to provide such data.

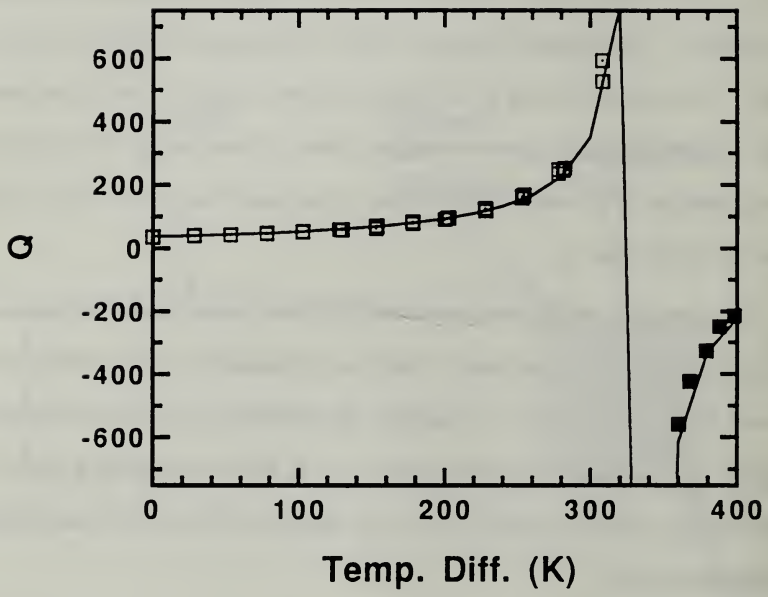

Figure 2 - Quality factor versus temperature difference for a helium-filled prime mover.

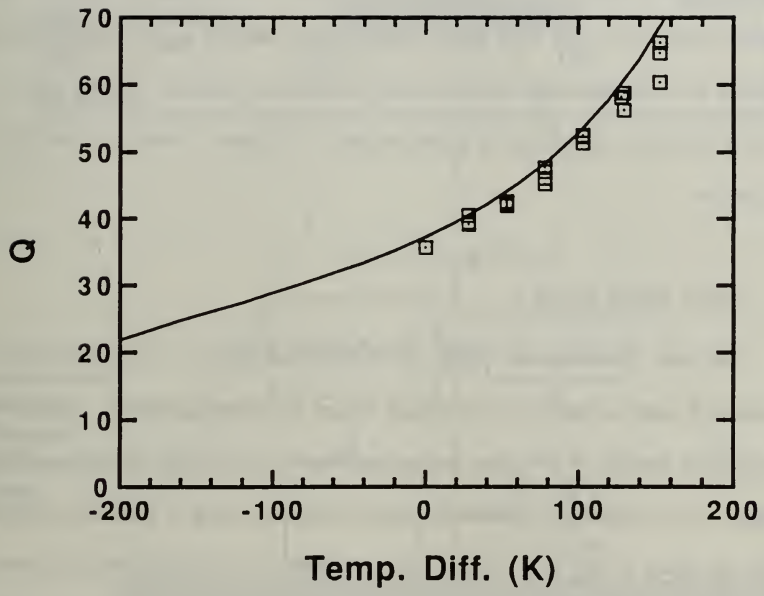

Figure 3 - Quality factor versus temperature difference extended to negative values of ΔT.

II. THEORY

The goal of this chapter is to provide the basic operating principle of a thermoacoustic muffler and to summarize the theory to be used in its analysis. The analysis method is, with only minor modifications, identical to the standing wave analysis of a thermoacoustic prime mover published by Professor Atchley [Ref. 3]. Only the important points will be presented here. The reader is referred to Ref. 3 for full details.

A. BASIC PRINCIPLES

The basic thermoacoustic effect is illustrated in Fig. 4. A poorly thermally conducting plate is situated near the rigid end of an acoustic resonator. There is a temperature gradient in the plate, so the temperature of the plate changes along its length. If the temperature gradient is positive, the temperature at the left end of the plate (as shown in Fig. 4) is less than that at the right. As we established an acoustic standing wave inside the tube, our attention will be on the oscillations of a parcel of gas located close to the surface of the plate, in other words, within about a thermal penetration depth of the plate. The equilibrium temperature of the parcel is T_m and the peak acoustic displacement of the parcel is ξ. Viscous effects are neglected in this elementary discussion, although they are included in the calculations. Also, to avoid issues of timing, we assume that the transition from compression to expansion, and vice versa, is instanteneous. Further, we assume the reduced or increased pressure is

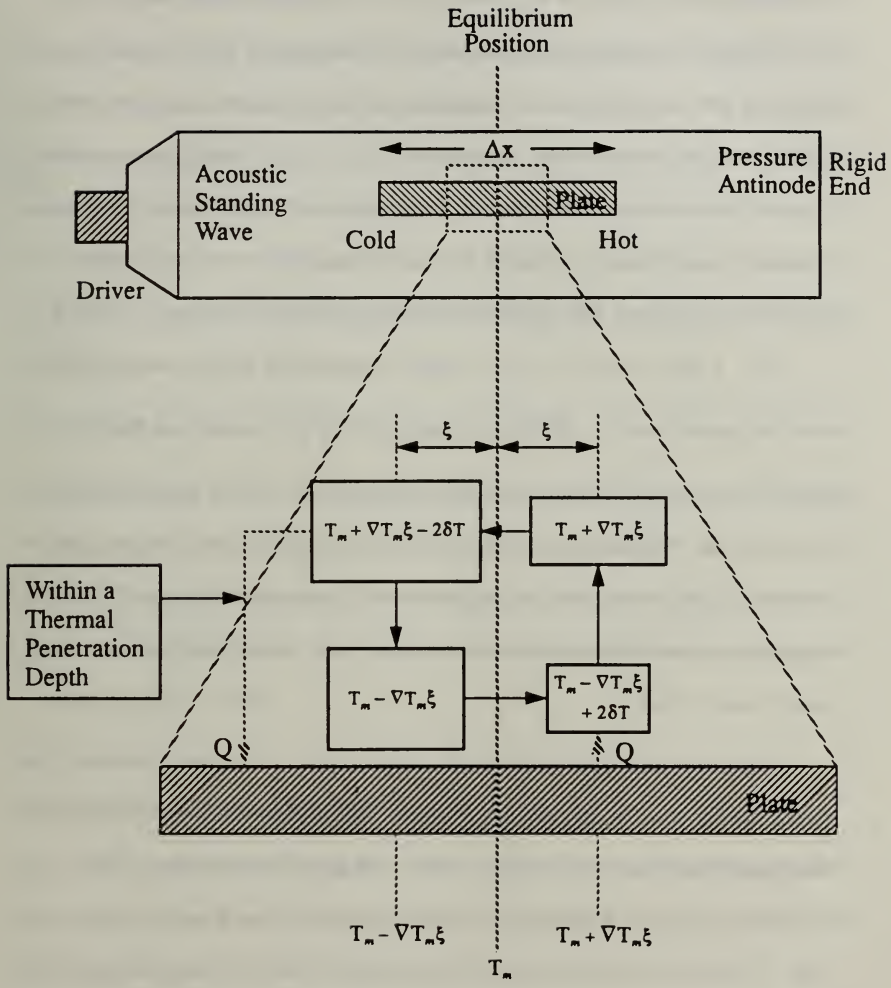

Figure 4 - A simplified illustration of the thermoacoustic effect.

held constant long enough for all thermal processes to achieve equilibrium.

We begin our observations just before the compression phase of the acoustic cycle. At this point the parcel is located above, and in thermal equilibrium with, a portion of the plate whose local temperature is $T_m - \nabla T_m \xi$. During the compression phase of the acoustic cycle the parcel is compressed and displaced toward the nearest acoustic pressure antinode, which is assumed to be located at the rigid end of the resonator in this case. The temperature of the parcel increases from $T_m - \nabla T_m \xi$ to $T_m - \nabla T_m + 2\delta T$, where $2\delta T$ is the change in temperature of the parcel due to the acoustic pressure change. If ∇T_m is greater than $\frac{\delta T}{\xi}$, when the parcel reaches its right-most excursion, the local temperature of the plate $T_m + \nabla T_m \xi$ will be higher than that of the gas. This temperature difference will cause a flow of heat from the plate to the parcel. Given enough time, the temperature of the parcel reaches $T_m + \nabla T_m \xi$. The important outcome of this portion of the acoustic cycle is that heat flows into the gas parcel when it is hot.

During the expansion phase of the acoustic cycle, the pressure decreases; the parcel moves back to the left and expands. As a result of this expansion, the temperature decreases to $T_m + \nabla T_m \xi - 2\delta T$. The parcel's temperature is higher than the local temperature of the plate ($T_m - \nabla T_m \xi$) and heat flows from the parcel to the plate. Eventually the parcel will come into equilibrium with the plate, at which point the parcel is returned to its initial state. That is, the parcel has undergone a complete thermodynamic cycle, just as the working substance in a conventional heat engine. The important outcome of the expansion phase of the cycle is that heat is removed

from the parcel when it is cold.

The phasing of the heat flow in the preceding discussion is the same as would be encountered in a conventional prime mover, as illustrated in Fig. 5. This figure shows the division of heat engines into two classes - prime movers and heat pumps - according to their mode of operation. In a prime mover, the engine takes heat in from a hot heat reservior, converts part of this heat into work, and rejects the remainder into a cold heat reservoir. In thermoacoustic heat transport, the parcel of gas is the engine and the work output is in the form of sound.

Referring back to Fig. 4, if ∇T_m is less than $\frac{\delta T}{\xi}$, then the phasing of the heat flow is reversed and the cycle mimics a heat pump. Energy is taken out of the sound field to pump heat. This is the principle underlying thermoacoustic refrigerators. For those applications, the emphasis is on the heat flow. However, if one concentrates on the acoustic energy, it is clear that this cycle also describes a sound attenuation mechanism, or a muffler.

B. THEORETICAL ANALYSIS

The performance of the muffler will be analyzed in terms of its ability to reduce the quality factor Q of the resonator in which it is housed. The Q of a resonator can be expressed as

$$Q = \frac{\omega E_{st}}{\dot{E}_{tot\ lost}} \quad , \tag{1}$$

where ω is the angular frequency of the acoustic field, E_{st} is the energy stored in the

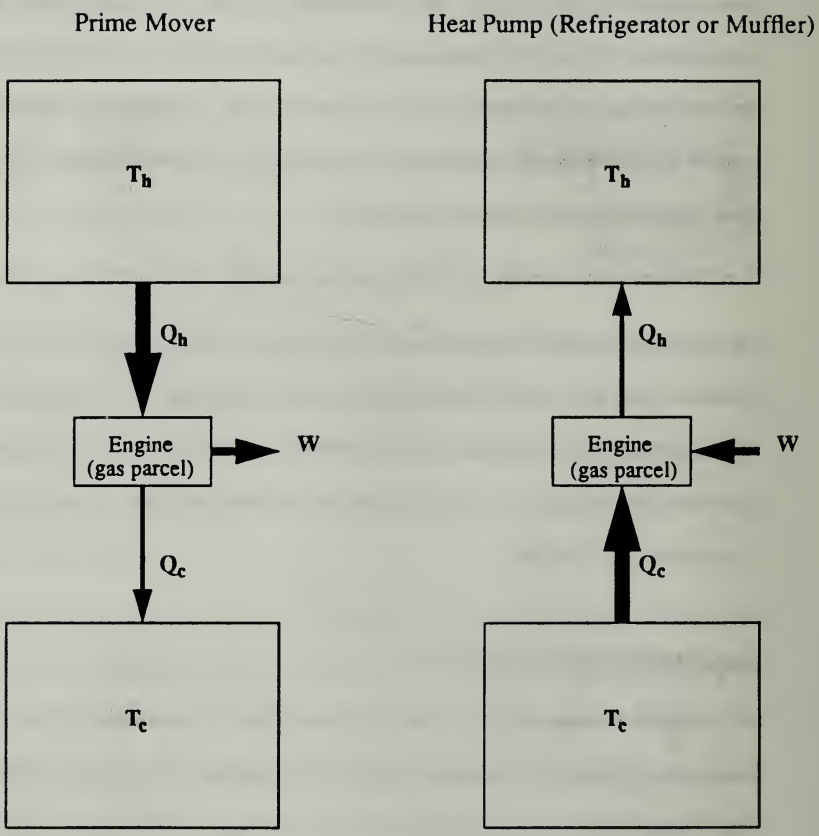

Figure 5 - Classical heat engine modes of operation.

resonator, and $\dot{E}_{tot\ lost}$ is the total acoustic power dissipated per cycle. The remainder of this chapter is devoted to a discussion of how E_{st} and $\dot{E}_{tot\ lost}$ are calculated.

As indicated in Fig. 6, the muffler is comprised of five major sections: the ambient end, the ambient heat exchanger, the muffler stack, the cold heat exchanger and the cold end. The power dissipated in the muffler is the sum of the power dissipated in each of these sections plus the power radiated out the open end.

$$\dot{E}_{tot\ lost} = \dot{E}_{amb\ end} + \dot{E}_{amb\ hx} + \dot{E}_{stack} + \dot{E}_{cold\ hx} + \dot{E}_{cold\ end} + \dot{E}_{rad} \quad . \tag{2}$$

The power dissipated in the five sections is found by integrating the power dissipated per unit surface area over the surface area of the resonator. Because complete details are provided in Ref. 3, they will be omitted here. The power radiated out the open end can be expressed as

$$\begin{aligned} \dot{E}_{rad\ lost} &= \frac{1}{2} R_{rad} u^2 \\ &= \frac{1}{2}\,\frac{1}{4}(k_{amb}R)^2 \rho_o c S\,\frac{P_A{}^2}{\rho_o{}^2 c^2} \\ &= \frac{1}{8}\,\frac{\pi R\,\omega P_A{}^2}{\rho_o c^2}\,k_{amb}R^3 \quad . \end{aligned} \tag{3}$$

The stored energy in the muffler is found by integrating the time-averaged acoustic density through out the entire volume of the muffler [Ref 3. Equation (24)].

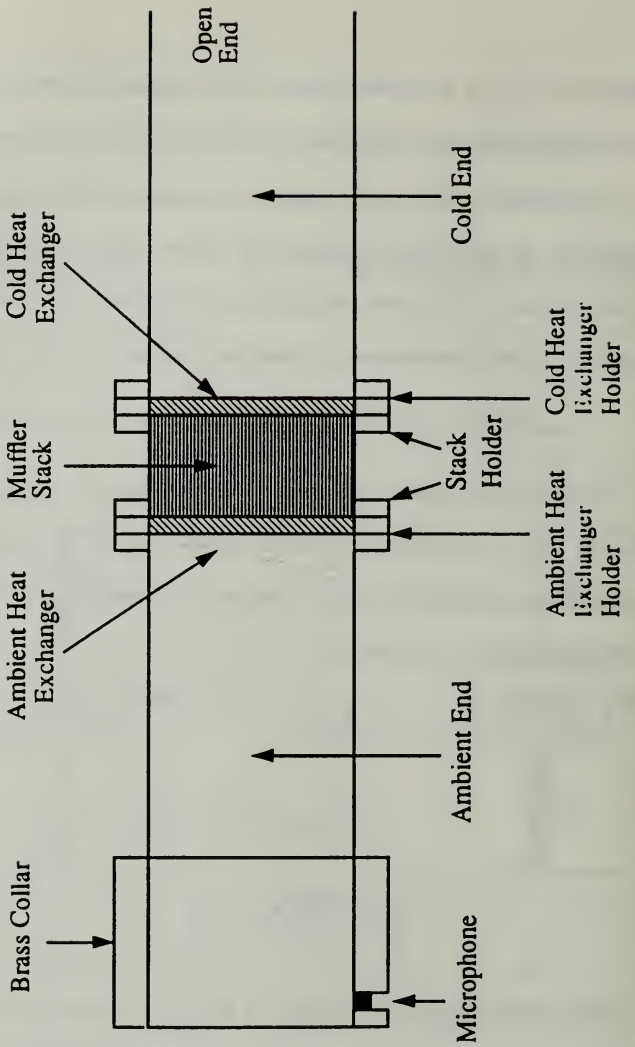

Figure 6 - A typical muffler configuration.

III. EXPERIMENT SETUP

The goal of this experiment is to measure the quality factor of a thermoacoustic muffler as a function of the temperature difference applied across the stack. The apparatus used to accomplish this goal is described in this chapter.

A. MUFFLER GEOMETRY

Figure 6 illustrates the physical construction of the muffler assembly. The tube is made from two 3.82 cm ID copper tubes, separated by the ambient heat exchanger, stack, and cold heat exchanger. The two sections of copper tube are 65.34 cm (ambient end) and 68.52 cm (cold end) long. One end of the ambient end is soldered to a brass collar. The purpose of the collar is to provide sufficient material to accomodate a microphone and to facilitate coupling to a piston driver. Both of these functions will be described below. The other end of the ambient end is soldered to a copper flange.

The copper flanges are designed to mate to the ambient and cold heat exchanger holders. Parallel plate, copper heat exchangers are soldered in the heat exchanger holders. The purpose of the heat exchangers is to maintain the corresponding end of the stack at the proper temperature. The ambient heat exchanger, as shown in Fig. 7, consists of 49, 0.254 mm (0.010 inch) thick, 8.22 mm long copper plates. The plates are spaced by 0.508 mm (0.020 inch). The total perimeter of the heat exchanger is 298.420 cm. The cold heat exchanger is very similar to the ambient heat

$\Pi = 2.9842$ m
$\Delta x = 8.22$ mm

Figure 7 - The ambient heat exchanger.

exchanger. The number, length, thickness and spacing of the plates in the two heat exchangers are identical. The only difference is in the perimeter. The perimeter of the cold heat exchanger is 295.826 cm.

The heat exchanger holders are designed to mate to the stack holder. To insure a tight fit, an o-ring groove is machined into the ambient end flange and ambient heat exchanger holder. Because the cold end will be subjected to low temperatures, o-ring seals will not work. The cold end flange, cold heat exchanger holder and cold stack holder flange are polished to provide a very smooth surface. Two 0.254 mm (0.010 inch) thick teflon sheets are positioned between these parts to provide the seal.

The stack holder is a 25.90 mm long, 37.22 mm ID stainless steel tube. The wall thickness is 0.535 mm. Each end of the tube is hard soldered to a stainless steel

flange. The flange is drilled and tapped to match bolt circles drilled in the ambient and cold end flanges and the two heat exchanger holders. The muffler stack fits inside the stack holder.

The stack is a spiral of 0.102 mm (0.004 inch) thick mylar spaced by 0.864 mm (0.034 inch) diameter monofilament fishing line which is glued to the mylar. The fishing line, spaced by approximately 5 mm, insures that a consistent spacing in maintined between the layers of mylar when it is wound into the spiral. The mylar is wound around a 6.35 mm (0.25 inch) diameter phenolic rod.

When fully assembled the total length of the muffler is 139.5 cm. Appendix A has a complete listing of the specifications of the geometrical parameters of the muffler.

B. EQUIPMENTAL SETUP

The experimental set up is shown in Fig. 8. Its function can described in terms of three major sections - temperature control, acoustic analysis, and gas handling.

1. Temperature Control Section

To establish a temperature difference across the stack, the cold end is cooled below room temperature with liquid nitrogen. To accomplish this cooling, the cold end is enclosed in a styrofoam box. The heat exchanger end and the open end of the cold end extend out the sides of the box. Tin loaf pans are placed at the bottom of the box. These pans provide a leak proof means of holding the liquid nitrogen. Approximately 20 short pieces of thick copper wire are secured to the cold end with

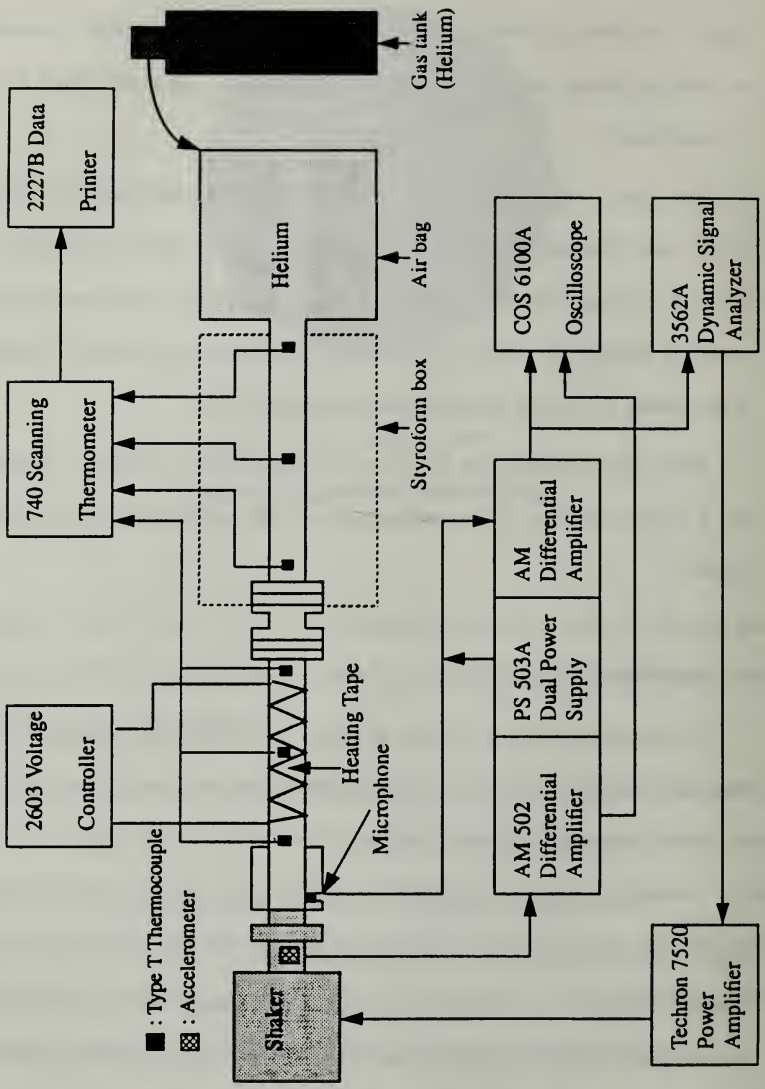

Figure 8 - Schematic diagram of the experimental setup for generating finite-amplitude standing waves.

hose clamps and extend down into the pans. These pieces of wire act as cold fingers to conduct heat from the cold end to the liquid nitrogen.

When the cold end is cooled, the ambient end tends to cool off because of thermal conduction through the stack and stack holder. To prevent this unwanted cooling and maintain the ambient end near room temperature, the ambient end is wrapped with heating tape. Electrical power is fed to the heating tape through a variable AC transformer. The transformer is adjusted to maintain the ambient end at the desired temperature.

The temperature of the muffler is monitored by six Type-T (copper-constantan) thermocouples. The thermocouples are located at the open end, middle and heat exchanger ends of the ambient and cold ends of the muffler. During operation, the ambient end temperature typically varies by less than approximately 2^{o}C along its length. The cold end temperature is not as uniform. The middle of the cold end is typically $10^{o} - 20^{o}$C colder than the two ends. In the calculations, the average temperature of each end is used to calculate the temperature difference across the stack. The output of the thermocouples is recorded with a Keithley 740 Scanning Thermometer.

2. Acoustic Analysis Section

The function of the acoustic analysis section is to measure the quality factor of the muffler. It consists of an acoustic driver, an accelerometer, a microphone, and a dynamic signal analyzer.

The drive signal is the source output of the HP 3562A dynamic signal analyzer. The periodic chirp mode is used to produce a swept sine wave signal. The signal is amplified with a Techron 7520 power amplifier and sent to a MB EA-1500 PM electrodynamic shaker. A 0.65 kg brass piston is mounted on the shaker. The piston diameter is 3.76 cm, slightly less than the ID of the muffler. A thin, natural rubber sheet (CENCO Part 18095-01) is streched across the end of the brass collar. Vacuum grease provides an air tight seal between the rubber diaphragm and the collar. The piston is positioned at the ambient end. The face of the piston is machined with a slight curvature to insure that no air is trapped between it and the diaphragm. The piston motion is monitored with an Endevco Type 2215 accelerometer. The shaker/piston is carefully aligned to minimize distortion in the accelerometer signal.

The sound field inside the muffler is monitored with a 0.594 cm diameter Endevco Model 8510B-5 piezoresistive pressure transducer. This microphone is mounted 4.21 mm from the end of the brass collar. The microphone output is amplified with at Tektronix AM 502 differential amplifier and sent to the signal analyzer.

3. Gas Handling Section

The muffler is filled with helium gas at a pressure just slightly above atmospheric. Helium gas was used to avoid water vapor, which forms frost inside the cold end. The open end of the cold end is coupled to a large trash bag. The purpose of this bag is to simulate an open end, yet allow the use of helium. In practice, the mufler is not immune to gas leaks. However, the amount of leakage was deemed

acceptable for our purposes.

C. DATA ACQUISITION

Prior to data acquisition the muffler cold end was cooled with liquid nitrogen. The lowest practical cold end temperature was approximately - 120^{o}C. Once the cold end had reached its lowest temperature, data acquisition began. As the cold end temperature slowly began to rise, a series of Q measurements were made until the cold end had come back to near room temperature. The initial cooling takes approximately one and one-half hours. The gradual warming takes aproximately three hours.

The Q is determined from a curve fit to the frequency response. The measurement of the frequency response and the curve fitting is performed by the dynamic signal analyzer. The curve fit provides a pole/zero analysis of the response. The parameters are given in the form a + j b. The resonance frequency f_o and Q are determined from the following equations

$$f_o = \sqrt{b^2 + a^2} \sim b \quad . \tag{4}$$

$$Q = \frac{\sqrt{b^2 + a^2}}{-2a} \sim \frac{-b}{2a} \quad . \tag{5}$$

IV. RESULTS AND DISCUSSION, SUMMARY AND RECOMMENDATIONS

The quality factor of the muffler was measured as a function of the temperature difference applied across the stack. The results of these measurements are presented and discussed in this chapter. The chapter concludes with a summary and recommendations for future work.

A. RESULTS AND DISCUSSION

The muffler is configured with one open end and one closed. Therefore, the resonance frequencies obey the equation

$$f_n = \frac{(2n - 1)}{4 L_{eff}} c \quad . \tag{6}$$

The stack is located at the approximate middle of the resonator. This placement dictates that the stack will attenuate sound in the resonator when it is excited at its second longitudinal mode.

Figure 9 shows the results of the measurements of Q as a function of the temperature difference across the stack. The data points represent five difference data sets. The solid line is the prediction of the standing wave analysis. The average stack temperature has been used to calculate the thermophysical properties of the gas in the stack. This assumption greatly simplifies the calculations and has been shown to yield reasonably accurate results. [Ref. 3] As the figure indicates, the data follow the same trend as the prediction and both show approximately the same percent reduction in Q.

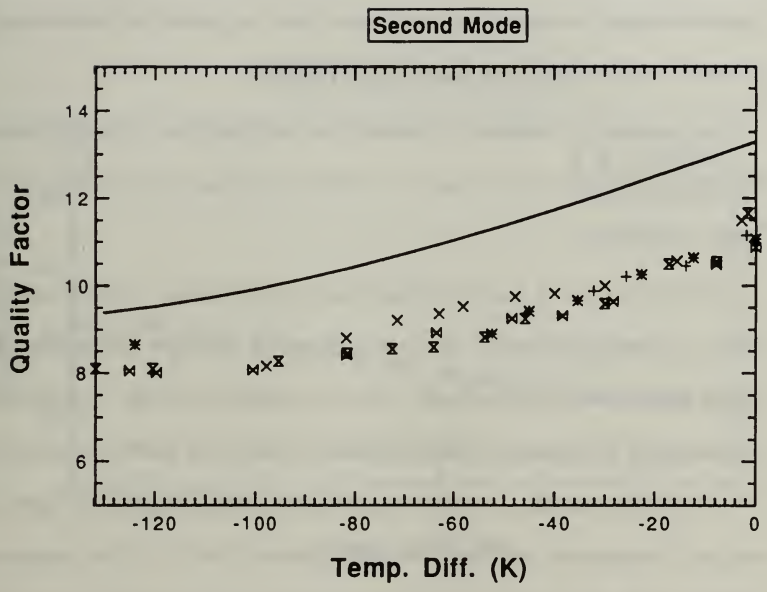

Figure 9 - Quality factor versus temperature difference for second mode.

The measured reduction in Q is approximately 30%. One cause for the discrepancy is that the gas inside the muffler is not pure helium, but a mix of helium and air. Evidence for this conclusion is the fact that the measured resonance fequencies were always less than those predicted for pure helium. Because the purpose of this thesis is a proof-of-concept experiment, no attemp was made to perform the calculations for mixtures of helium and air or to prevent small gas leaks.

The measured Q-reduction is certainly not adequate for a practical muffler. However, it does show that Q-reduction is possible and gives some encouragement for further investigation.

The combination of stack placement and the open-closed resonator geometry, results in an interesting feature. The even modes of the tube show Q-reduction while the odd modes show Q-enhancement. This point is borne out in Fig. 10 which shows the measured Q of the first and third longitudinal modes of the muffler as functions of ΔT. The Q-enhancement of the first mode is large enough that it in fact goes into onset at a temperature difference of approximately -130^{o} C. The spontaneous oscillation of the first mode is the reason that larger temperature differences were not used in the measurements of Q-reduction in the second mode. It should be noted that the muffler could have been designed so that the first mode showed Q-reduction, so onset of self-oscillation would not have limited the temperature range. However, this would have resulted in a cumbersomely long tube. Again, because we are interested only in proof of concept, we accepted this limitation.

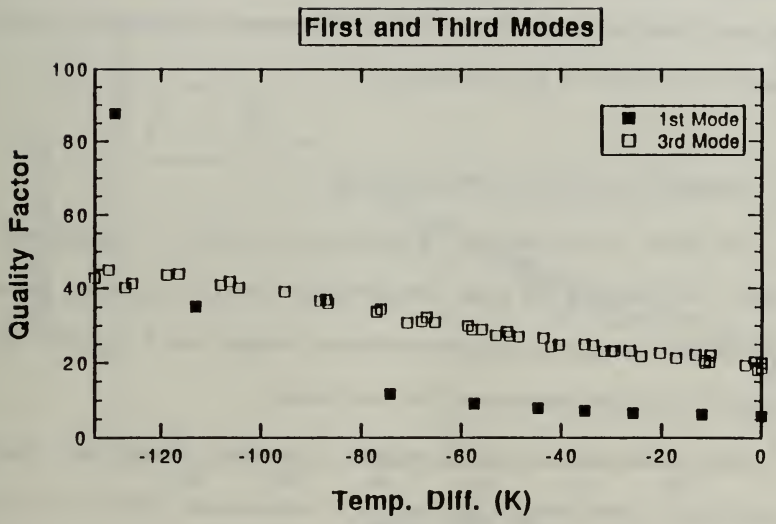

Figure 10 - Quality factor versus temperature difference for first mode and third mode.

The measurements in the previous figure indicate that the Q for the third mode tends to reach some limiting value, or perhaps even begins to decrease at large temperature differences. Fig. 11 shows the data for the third mode along with the predicted Q. Although there is some discrepancy as with the second mode, the measured behavior shows the same trends as the predicted bahavior. The Q is predicted to begin to decrease at larger values of temperature difference. The physical reason for this behavior is not completely clear.

B. SUMMARY AND RECOMMENDATIONS

The results of this thesis can be summarized as follows. A thermoacoustic muffler was constructed and tested. Measurements of the Q of a (mostly) helium filled muffler were made for temperature differences ranging from 0 to -130^{o}C. The expected Q-reduction, approximately 30%, was observed.

These results incidate that Q-reduction is possible. Future work should concentrate on optimization, to determine if a thermoacoustic muffler is, in fact, practical.

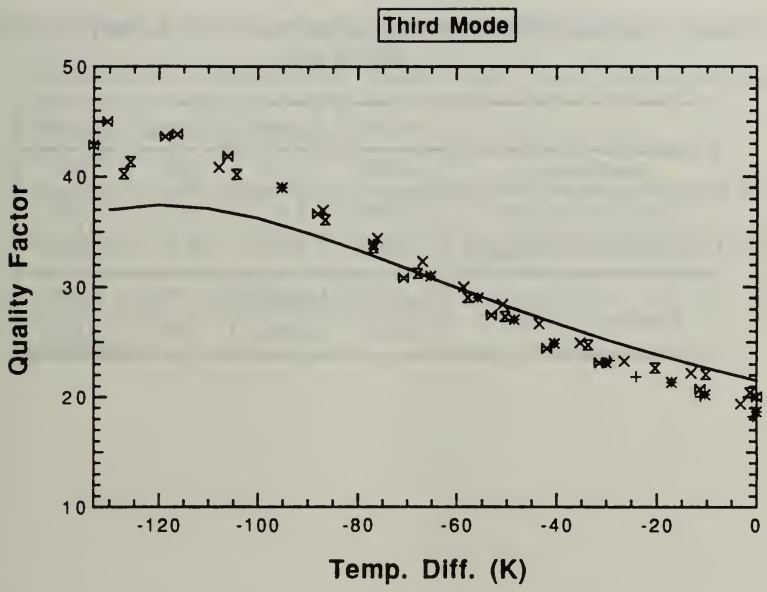

Figure 11 - Quality factor versus temperature difference for third mode.

APPENDIX A. LISTING OF THE SPECIFICATIONS OF THE GEOMETRICAL PARAMETERS OF THE MUFFLER

Table 1: SPECIFICATIONS OF THE GEOMETRICAL PARAMETERS OF THE MUFFLER

	Π (m)	Δx (mm)	l (mm)	y_0 (mm)
Muffler Stack	1.14193	25.74	0.05	0.43
Cold Heat Exchanger	2.95286	8.22	0.13	0.26
Ambient Heat Exchanger	2.98420	8.22	0.13	0.26
Parameters of Muffler	L_{amb} (m)	L_{cold} (m)	L (m)	R (m)
	0.6534	0.6852	1.395	0.0191

LIST OF REFERENCES

1. Lin, Hsiao-Tseng, "Investigation of a Heat Driven Thermoacoustic Prime Mover," Master's Thesis, Naval Postgraduate School, Monterey, California, December 1989.

2. Earl Clayton Bowers, "Investigation of Heat Driven Thermoacoustic Prime Mover Above Onset of Self-Oscillation," Master's Thesis, Naval Postgraduate School, Monterey, California, September 1991.

3. Anthony A. Atchley, "Standing Wave Analysis of a Thermoacoustic Prime Mover Below Onset of Self-Oscillation," *J. Acoustic. Soc. Am.* 92(5), 2907-2914 (1992).

4. G. W. Swift, "Thermoacoustic Engines," *J. Acoustic. Soc. Am.* 84, 1145-1180(1988).

INITIAL DISTRIBUTION LIST

		No. Copies
1.	Defense Technical Information Center Cameron Station Alexandria, Virginia 22304-6145	2
2.	Library, Code 52 Naval Postgraduate School Monterey, California 93943-5100	2
3.	Prof. Anthony A. Atchley, Code PH/Ay Department of Physics Naval Postgraduate School Monterey, California 93943	5
4.	Dr. Felipe Gaitan Department of Physics Naval Postgraduate School Monterey, California 93943	1
5.	CDR Che, Chun-Hua No.61 Kong-Ming Road, Chia-Yi, Taiwan R.O.C.	1
6.	LT Kuo, Fan-Ming No. 57-28 Ming-Fu Road, Pu-Li, Nen-Tou County, Taiwan R.O.C.	1

7. Library of Chinese Naval Academy 2

P.O. Box 8494 Tso-Ying, Kaohsiung, Taiwan

R.O.C.

8. Library of Chung-Cheng Institute of Technology 1

Tashih, Tao-Yuan, Taiwan

R.O.C.